mathematics

MDPI

Article

Nonlinear Mixed Convective Flow over a Moving Yawed Cylinder Driven by Buoyancy

Prabhugouda M. Patil [1,2], Hadapad F. Shankar [1] and Mikhail A. Sheremet [3,4,*]

[1] Department of Mathematics, Karnatak University, Pavate Nagar, Dharwad 580003, India; pmpmath@gmail.com (P.M.P.); shankarhf@gmail.com (H.F.S.)
[2] Pavate Institute of Mathematical Sciences (PMISci), Karnatak University, Pavate Nagar, Dharwad 580003, India
[3] Laboratory on Convective Heat and Mass Transfer, Tomsk State University, 634045 Tomsk, Russia
[4] Butakov Research Center, National Research Tomsk Polytechnic University, 634050 Tomsk, Russia
* Correspondence: sheremet@math.tsu.ru

Abstract: The fluid flow over a yawed cylinder is useful in understanding practical significance for undersea applications, for example, managing transference and/or separation of the boundary layer above submerged blocks and in suppressing recirculating bubbles. The present analysis examines nonlinear mixed convection flow past a moving yawed cylinder with diffusion of liquid hydrogen. The coupled nonlinear control relations and the border restrictions pertinent to the present flow problem are nondimensionalized by using nonsimilar reduction. Further, implicit finite difference schemes and Quasilinearization methods are employed to solve the nondimensional governing equations. Impact of several nondimensional parameters of the analysis on the dimensionless velocity, temperature and species concentration patterns and also on Nusselt number, Sherwood number and friction parameter defined at the cylinder shell is analyzed through numerical results presented in various graphs. Velocity profiles can be enhanced, and the coefficients of friction at the surface can be reduced, for increasing values of velocity ratio parameters along chordwise as well as spanwise directions. Species concentration profile is reduced, while the Sherwood number is enhanced, for growth of the Schmidt number and yaw angles. Furthermore, for an increasing value of yaw angle, skin-friction coefficient in chordwise direction diminishes in opposing buoyancy flow case, whereas the results exhibit the opposite trend in assisting buoyancy flow case. Moreover, very importantly, for increasing magnitude of nonlinear convection characteristic, the liquid velocity and surface friction enhance in spanwise direction. Further, for increasing magnitude of combined convection characteristics, velocity profiles and coefficient of friction at the surface enhance in both spanwise and chordwise directions. Moreover, we have observed that there is no deviation for zero yaw angle in Nusselt number and Sherwood number.

Keywords: mixed convection; yawed cylinder; double diffusion; nonlinear convection; quasilinearization technique

Citation: Patil, P.M.; Shankar, H.F.; Sheremet, M.A. Nonlinear Mixed Convective Flow over a Moving Yawed Cylinder Driven by Buoyancy. *Mathematics* **2021**, *9*, 1275. https://doi.org/10.3390/math9111275

Academic Editor: Ana-Maria Acu

Received: 4 May 2021
Accepted: 28 May 2021
Published: 1 June 2021

1. Introduction

Many researchers over the last few decades have given considerable attention to the investigation of heat and mass transfer characteristics of combined convection in various flow geometries. Combined convection flows appear when the temperature and species concentration variations between the wall and the external liquid are larger and, hence, become important when buoyancy forces significantly disturb the circulation, heat and species concentration patterns. When the fluid is subjected to two various density drops having various rates of diffusion, it is meant to be the double diffusion convection. The density differences may be caused by gradients in the liquid concentration, or by the changes in the temperature. The double diffusive mixed convection plays a vital role in boundary layer flow problems because of its significance in several technical and

geophysical challenges including solar collectors, solar ponds, lakes, reservoirs and crystal growth [1]. Due to its vast applications, many researchers have worked on the double diffusion combined convection flow past various geometries such as sphere, exponential stretching sheet, vertical cone, slender cylinder, moving plate, etc. [2–7].

However, for viscous liquid flows with heat transfer, the impact of linear dependence of density on dimensionless temperature, that is, natural convection, seems to be highly significant in applications pertaining to industrial manufacturing processes and, therefore, cannot be ignored. The "temperature and density relation" is nonlinear for a large distinction between the border and liquid temperatures, the nonlinear density temperature differences in the buoyancy force term have a substantial effect on the circulation and energy transference features. Vajravelu and Sastri [8] have analyzed the heat transfer characteristics between the vertical borders with and without the nonlinear density temperature differences. Bhargav and Agarwal [9] have examined the fully developed free convection with temperature-dependent density within a duct. Mosta et al. [10] have examined the influence of nonlinear temperature combined with density differences in nanosuspension convection over a vertical border. In the present analysis, the "nonlinear temperature and density relation" is regarded owing to the important variation between the liquid and wall temperatures. At the same time, the liquid hydrogen diffusion [3,5] is regarded because of its cooling ability.

The boundary layer concept is the most useful and important aspect in understanding the transport processes occurring in external flows. The phenomenal results of the mixed convection flow along various geometries have been contributed by various researchers around the globe. Recently, Muthukumaran and Bathinathanan [11] have worked on mixed convection boundary layer flow over a stretching sheet, and their results have revealed that the heat transfer rate increases with a raise of the Prandtl number for both assisting and opposing flows. Halim and Noor [12] have analyzed mixed convection over a vertical stretching sheet, and their outcomes have revealed that the assisting flow has higher rates of heat and mass transfer compared to the opposing flow. Alsabery et al. [13] have investigated the mixed convection through a rotating cylinder. Khashiie et al. [14] have worked on mixed convection flow over a Riga plate. Complex flow patterns over yawed cylindrical cables, suppression of fluctuations in lift forces and the control of the drag forces are the main problems encountered in the engineering design. At the same time, the investigation of combined convection circulation about a tilted cylinder has not been analyzed so far. The examination of motion along tilted cylinder is very useful for heat exchangers design [15]. The fluid flow past yawed and unyawed cylindrical geometries extensively occurs in various engineering-related applications, like tow cables, chimney stacks, different towers, sub-sea pipelines, risers, heat exchangers and overhead cables [16,17]. King [16] has studied the vortex exited oscillations of yawed circular cylinders. This study reveals that the sustained oscillations can be observed at the yaw angles ranging between $\pm 65^{\circ}$. Najafi et al. [18] have studied the undisturbed flows over the yawed cylinder, wherein it is observed that eddies near the wake of the cylinder detach due to the increase in the angle of yaw. Further, Snarski [19] has investigated the variation of wall pressure on circular cylinder due to yaw angle and has revealed that the spectra exhibit powerful narrow band energy stages related with the Strouhal vortex shedding region, for the degrees of yaw angle ranging from $\pi/3$ to $\pi/2$. In the work of Sears [20], the boundary layer motion along a yawed cylinder is analyzed, and it is noticed that the location of the boundary layer separation point is independent from the yaw angle. Moreover, Thapa et al. [21] have investigated numerically the circulation over a yawed circular cylinder near the plane border. In the work of Gupta and Sarma [22], the time-dependent circulation along a yawed infinite cylinder under the influence of cross flow has been analyzed, and this analysis reveals that the coefficient of friction along chordwise direction diminishes with larger values of nonsimilar variable (ξ). Further, Bucker and Lueptow [23] have examined the boundary layer flow on weakly yawed cylinders, and they have found that the thickness of boundary layer rises nonlinearly for small degree

yaw angle. In this direction, many of the researchers have worked on the boundary layer flow past a yawed cylinder with the influence of non-uniform suction/injection [17,24–27]. Marshall [28] has studied the disturbed flow along a moving yawed cylinder and found that, as cross stream Reynolds number increases, the surface vorticity enhances. Vakil and Green [29] have performed numerical calculations pertaining to the flow over a yawed cylinder for moderate values of Reynolds number, i.e., $1 \leq Re \leq 40$, and have validated the independence principle and also proposed an empirical relation for the lift and drag forces on the cylinder. Recently, Patil et al. [30] have scrutinized the combined convection circulation along a yawed cylinder, and the obtained data reveal that the liquid velocity and surface drag coefficient at the cylinder's boundary in all directions rises with the heat transfer rate because of combined convection.

From the above literature review, it is found that the investigation of double diffusive combined convection past a moving yawed cylinder has not been attempted so far. Since, many authors such as Roy [25], Chiu and Lienhard [31], Roy and Saikrishnan [26] and Revathi et al. [17] have analyzed a boundary layer flow over a yawed cylinder. The works of these researchers have stimulated us to work on the present article, and, therefore, we have scrutinized the considered challenge. However, the present problem is formulated as an endeavor to investigate the steady combined convection boundary layer flow around a moving yawed cylinder. The novelty in the present analysis is as follows:

- Convective flow over a moving yawed cylinder driven by buoyancy.
- Influence of liquid hydrogen diffusion.
- Effects of yawed angle.
- Flow characteristics in chordwise and spanwise directions.

The considered governing equations and boundary conditions have been reduced using nonsimilar technique. Further, these equations are solved by employing the quasilinearization method and the implicit finite difference schemes [32–34].

2. Mathematical Simulation

Herein, we analyze the viscous, laminar, incompressible, combined convective flow over a moving yawed cylinder. The flow system is demonstrated in Figure 1, where the liquid (water) is supposed to move over a vertically yawed cylinder with radius R so that the yaw angle θ is used between 0 and $\pi/6$. Here, $\theta = 0$ represents the vertical cylinder, while $\theta = \pi/2$ represents the horizontal cylinder. To have the influence of buoyancy, the cylinder must be regarded in vertical or tilted location because the investigation is of combined convection. Therefore, the yaw angle is regarded in the range $0 \leq \theta \leq \pi/2$. The magnitude of angle of yaw above $\pi/6$ is not regarded because it would be nearer to stagnation point circulation and it is not the aim of the current examination of combined convection flow. For analysis, x and z are the coordinate axes in chordwise and spanwise directions, respectively, with u and w denoting the corresponding velocity components. Moreover, y is the coordinate axis drawn normal to x and z axes with v denoting the corresponding velocity component. The temperature and species concentration of the liquid at the border are denoted by T_s and C_s, while that away from the surface are represented by T_∞ and C_∞. The density changes are modeled using the Boussinesq approach [5,35].

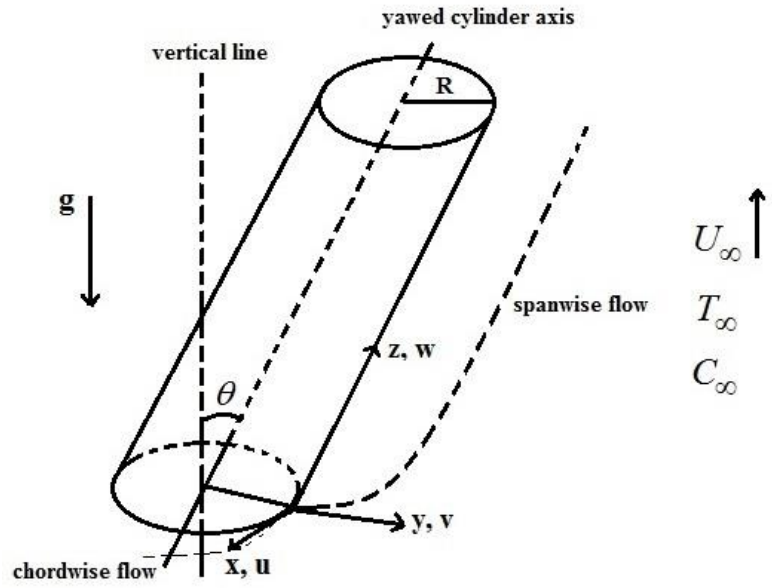

Figure 1. Sketch of the motion with coordinates.

The governing equations representing the fluid flow variations are as follows [17,24–27,30,36]

Continuity equation

$$\frac{\partial u}{\partial x} + \frac{\partial v}{\partial y} = 0 \tag{1}$$

Momentum equation along chordwise direction

$$\begin{aligned} u\frac{\partial u}{\partial x} + v\frac{\partial u}{\partial y} = u_e\frac{du_e}{dx} + g\left\{\beta_1(T-T_\infty) + \beta_2(T-T_\infty)^2\right\}\sin(\theta) \\ +\nu\frac{\partial^2 u}{\partial y^2} + g\left\{\beta_3(C-C_\infty) + \beta_4(C-C_\infty)^2\right\}\sin(\theta) \end{aligned} \tag{2}$$

Momentum equation along spanwise direction

$$\begin{aligned} u\frac{\partial w}{\partial x} + v\frac{\partial w}{\partial y} = \nu\frac{\partial^2 w}{\partial y^2} + g\left\{\beta_1(T-T_\infty) + \beta_2(T-T_\infty)^2\right\}\cos(\theta) \\ +g\left\{\beta_3(C-C_\infty) + \beta_4(C-C_\infty)^2\right\}\cos(\theta) \end{aligned} \tag{3}$$

Energy equation

$$u\frac{\partial T}{\partial x} + v\frac{\partial T}{\partial y} = \frac{k}{\rho c_p}\frac{\partial^2 T}{\partial y^2} \tag{4}$$

Concentration equation

$$u\frac{\partial C}{\partial x} + v\frac{\partial C}{\partial y} = D_B\frac{\partial^2 C}{\partial y^2} \tag{5}$$

The prescribed boundary conditions are

$$\left.\begin{array}{ll} y = 0: & u = u_s(x), \quad v = 0, \quad w = w_s(x), \quad C = C_s, \quad T = T_s, \\ y \to \infty: & u \to u_e(x) = 2u_\infty \sin\left(\frac{x}{R}\right), \quad w \to w_e = w_\infty\cos(\theta), \; C \to C_\infty, \; T \to T_\infty \end{array}\right\} \tag{6}$$

The nonsimilar transformations and the resulting variables are

$$\left.\begin{array}{l} \xi = \int_0^x \frac{u_e}{u_\infty}\, d\left(\frac{x}{R}\right), \eta = \left(\frac{Re}{2\xi}\right)^{\frac{1}{2}}\left(\frac{u_e}{u_\infty}\right)\frac{y}{R}, u_\infty = w_\infty\sin(\theta), \\ w = w_e \cdot S = w_\infty\cos(\theta)\cdot S, G = \frac{T-T_\infty}{T_s-T_\infty}, H = \frac{C-C_\infty}{C_s-C_\infty}, \\ \psi(x,y) = u_\infty R\left(\frac{2\xi}{Re}\right)^{\frac{1}{2}} f(\xi,\eta), u = \frac{\partial\psi}{\partial y}, v = -\frac{\partial\psi}{\partial x}, Re = \frac{\rho u_\infty R}{\mu} \end{array}\right\} \tag{7}$$

In view of (7), we have

$$u = 2u_\infty \sin\left(\tfrac{x}{R}\right) F$$
$$v = u_\infty \left\{ -\tfrac{y}{R}\left(2\cos\left(\tfrac{x}{R}\right) - \tfrac{\sin^2\left(\frac{x}{R}\right)}{1-\cos\left(\frac{x}{R}\right)}\right) F - \left(\tfrac{2}{\mathrm{Re}\cdot\xi}\right)^{\frac{1}{2}} f \cdot \sin\left(\tfrac{x}{R}\right) - 2\left(\tfrac{2\xi}{\mathrm{Re}}\right)^{\frac{1}{2}} \cdot \sin\left(\tfrac{x}{R}\right) f_\xi \right\}$$

Now, utilizing the transformations (7), Equations (2)–(5) can be written as

$$\begin{array}{l} F_{\eta\eta} + fF_\eta + \beta(\xi)\left(1 - F^2\right) + 2\xi(F_\eta f_\xi - FF_\xi) + \\ + Ri\, s(\xi)\{(1 + \beta_T G)G + (1 + \beta_c H)NcH\}\sin(\theta) = 0 \end{array} \tag{8}$$

$$S_{\eta\eta} + f \cdot S_\eta + 2\xi(S_\eta f_\xi - FS_\xi) + Rip(\xi)\{(1 + \beta_T G)G + (1 + \beta_c H)NcH\}\sin(\theta) = 0 \tag{9}$$

$$G_{\eta\eta} + Pr \cdot f \cdot G_\eta + 2\xi(G_\eta f_\xi - FG_\xi)Pr = 0 \tag{10}$$

$$H_{\eta\eta} + Sc \cdot f \cdot H_\eta + 2\xi(H_\eta f_\xi - FH_\xi)Sc = 0 \tag{11}$$

The employed boundary conditions are given below

$$\left.\begin{array}{llllll} \text{at} & \eta = 0: & F = \varepsilon_1, & S = \varepsilon_2, & G = 1, & H = 1, \\ \text{as} & \eta \to \infty, & F = 1, & S = 1, & G = 0, & H = 0 \end{array}\right\} \tag{12}$$

The nondimensional characteristics arising in this investigation are

$$\begin{array}{l} \beta(\xi) = \frac{\xi\cos(\overline{x})}{\sin^2(\overline{x})},\ Ri = \frac{g\beta_1(T_s - T_\infty)R}{u_\infty^2},\ s(\xi) = \frac{\xi}{4\sin^3(\overline{x})},\ Nc = \frac{\beta_3(C_s - C_\infty)}{\beta_1(T_s - T_\infty)}, \\ p(\xi) = \frac{\xi}{2\sin^2(\overline{x})},\ \beta_T = \frac{\beta_2(T_s - T_\infty)}{\beta_1},\ \beta_C = \frac{\beta_4(C_s - C_\infty)}{\beta_3},\ \text{where } \overline{x} = \frac{x}{R} \end{array} \tag{13}$$

Furthermore, $f(\xi,\eta) = \int_0^\eta F d\eta + f_s$; where $f_s = 0$ represents an impermeable yawed cylinder.

The velocity distribution is

$$u_e(\overline{x}) = 2u_\infty \sin(\overline{x}), w_e(\overline{x}) = w_\infty \cos(\theta) = \text{constant, where } \overline{x} = \frac{x}{R} \tag{14}$$

Therefore, ξ, $\beta(\xi)$, $s(\xi)$ and $p(\xi)$ can be defined in terms of $\overline{x}$

$$\begin{array}{l} \xi = 2[1 - \cos(\overline{x})],\ \beta(\overline{x}) = \frac{2\cos(\overline{x})}{1+\cos(\overline{x})}, \\ s(\overline{x}) = \frac{1}{2\sin(\overline{x})[1+\cos(\overline{x})]},\ p(\overline{x}) = \frac{1}{1+\cos(\overline{x})} \end{array} \tag{15}$$

Using the following relation, equations are expressed in $\overline{x}$ instead of ξ

$$\xi\frac{\partial}{\partial\xi} = B(\overline{x})\frac{\partial}{\partial\overline{x}} \tag{16}$$

$$\text{where } B(\overline{x}) = \tan\left(\frac{\overline{x}}{2}\right) \tag{17}$$

In view of Equations (16) and (17), Equations (8)–(11) become as follows

$$\begin{array}{l} F_{\eta\eta} + fF_\eta + \beta(\overline{x})\left(1 - F^2\right) + 2B(\overline{x})(F_\eta f_{\overline{x}} - FF_{\overline{x}}) + \\ + Ri \cdot\ s(\overline{x})\{(1 + \beta_T G)G + (1 + \beta_c H)NcH\}\sin(\theta) = 0 \end{array} \tag{18}$$

$$S_{\eta\eta} + f \cdot S_\eta + 2B(\overline{x})(S_\eta f_{\overline{x}} - FS_{\overline{x}}) + Ri \cdot p(\overline{x})\{(1 + \beta_T G)G + (1 + \beta_c H)NcH\}\sin(\theta) = 0 \tag{19}$$

$$G_{\eta\eta} + Pr \cdot f \cdot G_\eta + 2B(\overline{x})(G_\eta f_{\overline{x}} - FG_{\overline{x}})Pr = 0 \tag{20}$$

$$H_{\eta\eta} + Sc \cdot f \cdot H_\eta + 2B(\overline{x})(H_\eta f_{\overline{x}} - FH_{\overline{x}})Sc = 0 \tag{21}$$

The relevant boundary conditions are

$$\left.\begin{array}{llllll} \text{at} & \eta = 0 & F = \varepsilon_1, & S = \varepsilon_2, & G = 1, & H = 1, \\ \text{as} & \eta \to \infty & F = 1, & S = 1, & G = 0, & H = 0 \end{array}\right\} \tag{22}$$

Skin friction coefficient along chordwise direction can be defined as follows $C_f = \frac{2\left(\mu\frac{\partial u}{\partial y}\right)_w}{\rho w_\infty^2}$. Taking into account Equation (7) one can define this skin friction parameter as $C_f = \frac{2\mu\left(4\frac{u_\infty}{R}\sin^2(\overline{x})\left(\frac{Re}{2\xi}\right)^{0.5}F_\eta(\overline{x},0)\right)\sin^2(\theta)}{\rho u_\infty^2}$, $(u_\infty = w_\infty\sin(\theta))$ and as a result

$$\begin{array}{l} C_f = \frac{4(1+\cos(\overline{x}))(1-\cos(\overline{x}))^{0.5}\sin^2(\theta)F_\eta(\overline{x},0)}{Re^{0.5}}, \\ \text{i.e., } Re^{0.5}C_f = 4(1+\cos(\overline{x}))(1-\cos(\overline{x}))^{0.5}\sin^2(\theta)F_\eta(\overline{x},0) \end{array} \tag{23}$$

Skin friction coefficient along spanwise direction can be defined as follows $\overline{C}_f = \frac{2\left(\mu\frac{\partial w}{\partial y}\right)_w}{\rho w_\infty^2}$. Taking into account Equation (7) one can define this skin friction parameter as $\overline{C}_f = \frac{2\mu\left(2w_e\frac{\sin(\overline{x})}{R}\left(\frac{Re}{2\xi}\right)^{1/2}S_\eta(\overline{x},0)\right)\sin^2(\theta)}{\rho u_\infty^2}$, $(w_e = w_\infty\cos(\theta))$ and as a result

$$\overline{C}_f = \frac{2^{1.5}\cos\left(\frac{\overline{x}}{2}\right)\cos(\theta)\sin(\theta)S_\eta(\overline{x},0)}{Re^{0.5}}, \text{ i.e., } Re^{0.5}\overline{C}_f = 2^{1.5}\cos\left(\frac{\overline{x}}{2}\right)\cos(\theta)\sin(\theta)S_\eta(\overline{x},0) \tag{24}$$

Nusselt number reflecting the heat transfer rate can be defined as $Nu = -\frac{R\left(\frac{\partial T}{\partial y}\right)_w}{(T_w - T_\infty)}$. Taking into account Equation (7), one can find $Nu = -\frac{R\left((T_w-T_\infty)\frac{2\sin(\overline{x})}{R}\left(\frac{Re}{2\xi}\right)^{0.5}G_\eta(\overline{x},0)\right)}{(T_w-T_\infty)}$ and $Nu = -2\sin(\overline{x})\left(\frac{Re}{2\xi}\right)^{0.5}G_\eta(\overline{x},0)$. Using Equation (15) for ξ, one can find $Re^{-0.5}Nu = -\frac{\sin(\overline{x})}{(1-\cos(\overline{x}))^{1/2}}G_\eta(\overline{x},0)$ and $Re^{-0.5}Nu = -\left(\frac{2\sin\left(\frac{\overline{x}}{2}\right)\cos\left(\frac{\overline{x}}{2}\right)}{\sqrt{2}\cdot\sin\left(\frac{\overline{x}}{2}\right)}G_\eta(\overline{x},0)\right)$, where $(1-\cos(\overline{x})) = 2\cdot\sin^2\left(\frac{\overline{x}}{2}\right)$. As a result

$$Nu = \frac{-\sqrt{2}\cos\left(\frac{\overline{x}}{2}\right)G_\eta(\overline{x},0)}{Re^{-0.5}}, \text{ i.e., } Re^{-0.5}Nu = -\sqrt{2}\cos\left(\frac{\overline{x}}{2}\right)G_\eta(\overline{x},0) \tag{25}$$

Sherwood number reflecting the mass transfer rate can be defined as $Sh = -\frac{R\left(\frac{\partial C}{\partial y}\right)_w}{(C_w - C_\infty)}$. Taking into account Equation (7) one can find $Sh = -\frac{R\left((C_w-C_\infty)\frac{2\sin(\overline{x})}{R}\left(\frac{Re}{2\xi}\right)^{0.5}H_\eta(\overline{x},0)\right)}{(C_w-C_\infty)}$ and $Sh = -2\sin(\overline{x})\left(\frac{Re}{2\xi}\right)^{0.5}H_\eta(\overline{x},0)$. Using Equation (15) for ξ, one can find $Re^{-0.5}Sh = -\frac{\sin(\overline{x})}{(1-\cos(\overline{x}))^{0.5}}H_\eta(\overline{x},0)$ and $Re^{-0.5}Sh = -\left(\frac{2\sin\left(\frac{\overline{x}}{2}\right)\cos\left(\frac{\overline{x}}{2}\right)}{\sqrt{2}\cdot\sin\left(\frac{\overline{x}}{2}\right)}H_\eta(\overline{x},0)\right)$, where $(1-\cos(\overline{x})) = 2\cdot\sin^2\left(\frac{\overline{x}}{2}\right)$. As a result

$$Sh = \frac{-\sqrt{2}\cos\left(\frac{\overline{x}}{2}\right)H_\eta(\overline{x},0)}{Re^{-0.5}}, \text{ i.e., } Re^{-0.5}Sh = -\sqrt{2}\cos\left(\frac{\overline{x}}{2}\right)H_\eta(\overline{x},0) \tag{26}$$

3. Solution Technique

Equations (18)–(21) are linearized using quasilinearization technique as below

$$F_{\eta\eta}^{i+1} + A_1^i F_\eta^{i+1} + A_2^i F_{\overline{x}}^{i+1} + A_3^i F^{i+1} + A_4^i G^{i+1} + A_5^i H^{i+1} = A_6^i \tag{27}$$

$$S_{\eta\eta}^{i+1} + B_1^i S_\eta^{i+1} + B_2^i S_{\overline{x}}^{i+1} + B_3^i F^{i+1} + B_4^i G^{i+1} + B_5^i H^{i+1} = B_6^i \tag{28}$$

$$G_{\eta\eta}^{i+1} + C_1^i G_\eta^{i+1} + C_2^i G_{\overline{x}}^{i+1} + C_3^i F^{i+1} = C_4^i \tag{29}$$

$$H_{\eta\eta}^{i+1} + D_1^i H_\eta^{i+1} + D_2^i H_{\overline{x}}^{i+1} + D_3^i F^{i+1} = D_4^i \tag{30}$$

where the coefficients at the $(i+1)$th iteration are defined employing the known ith iterative parameters. The dimensionless boundary conditions are

$$\left.\begin{array}{llll} F^{i+1} = \varepsilon_1, & S^{i+1} = \varepsilon_2, & G^{i+1} = 1, & H^{i+1} = 1 \quad \text{at } \eta = 0, \\ F^{i+1} = 1, & S^{i+1} = 1, & G^{i+1} = 0, & H^{i+1} = 0 \quad \text{at } \eta = \eta_\infty \end{array}\right\} \tag{31}$$

where the boundary layer edge is denoted by η_∞.

The coefficients in Equations (27)–(30) are given below

$$\begin{array}{l} A_1^i = f + 2B(\overline{x})f_{\overline{x}}, A_3^i = -2B(\overline{x})F, A_3^i = -2\beta(\overline{x})F - 2B(\overline{x})F_{\overline{x}}, \\ A_4^i = Ri \cdot s(\overline{x})(1 + 2\beta_T G)\sin(\theta), A_5^i = Ri \cdot s(\overline{x})(1 + 2\beta_C H)Nc\sin(\theta), \\ A_6^i = -2B(\overline{x})FF_{\overline{x}} - \beta(\overline{x})\left(1 + F^2\right) + Ri \cdot s(\overline{x})\left(\beta_T G^2 + Nc\beta_C H^2\right)\sin(\theta), \\ B_1^i = f + 2B(\overline{x})f_{\overline{x}}, B_2^i = -2B(\overline{x})F, B_3^i = -2B(\overline{x})S_{\overline{x}}, \\ B_4^i = Ri \cdot p(\overline{x})(1 + 2\beta_T G)\sin(\theta), B_5^i = Ri \cdot p(\overline{x})(1 + 2\beta_C H)Nc\sin(\theta), \\ B_6^i = -2B(\overline{x})FS_{\overline{x}} + Ri \cdot p(\overline{x})\left(\beta_T G^2 + Nc\beta_C H^2\right)\sin(\theta), \\ C_1^i = Pr(f + 2B(\overline{x})f_{\overline{x}}), C_2^i = -2PrB(\overline{x})F, C_3^i = -2PrB(\overline{x})G_{\overline{x}}, C_4^i = -2PrB(\overline{x})FG_{\overline{x}}, \\ D_1^i = Sc(f + 2B(\overline{x})f_{\overline{x}}), D_2^i = -2ScB(\overline{x})F, D_3^i = -2ScB(\overline{x})H_{\overline{x}}, D_4^i = -2ScB(\overline{x})FH_{\overline{x}} \end{array}$$

The nonlinear coupled partial differential Equations (18)–(21) under the boundary conditions (22) have been solved numerically using an implicit finite difference scheme in combination with the quasilinearization technique. The quasilinearization technique can be viewed as a generalization of the Newton–Raphson approximation method in functional space. An iterative sequence of linear equations is carefully constructed to approximate the nonlinear Equations (18)–(21) under the boundary conditions (22) achieving quadratic convergence and monotonicity. Applying the quasilinearization technique, the nonlinear coupled partial differential Equations (18)–(21) with boundary conditions (22) are replaced by the sequence of linear ordinary differential equations. Because the method is presented for ordinary differential equations by Inouye and Tate [37] and for partial differential equations in a recent study by Singh and Roy [38], its detailed description is not provided here. At each iteration step, the sequence of linear partial differential Equations (27)–(30) is expressed in difference form using the central difference scheme in the $\overline{x}$-direction and the backward difference scheme in η direction. Thus, in each step, the resulting equations have been then reduced to a system of linear algebraic equations with a block tri-diagonal matrix, which is solved by Varga's algorithm [39]. To ensure the convergence of the numerical solution to the exact solution, step sizes $\Delta\overline{x}$ and $\Delta\eta$ are taken as 0.01 and 0.01. A convergence criterion based on the relative difference between the current and previous iteration values is employed. When the difference reaches 0.0001, the solution is assumed to have converged and the iteration process is terminated, i.e., $\max\left\{\left|(F_\eta)_s^{i+1} - (F_\eta)_s^i\right|, \left|(G_\eta)_s^{i+1} - (G_\eta)_s^i\right|, \left|(H_\eta)_s^{i+1} - (H_\eta)_s^i\right|, \left|(S_\eta)_s^{i+1} - (S_\eta)_s^i\right|\right\} \leq 10^{-4}$.

4. Results and Discussion

In order to examine the qualitative behavior of fluid flow characteristics over a moving yawed cylinder, comprehensive numerical computation has been carried out for numerous values of nondimensional parameters that characterize the flow, heat and mass transfer. The simulated outcomes are presented graphically. Considering water as the working liquid, the value of Prandtl number $Pr = 7$ is selected. The realistic Schmidt numbers are $Sc = 160$, 240 and 340 which correspond to liquid hydrogen, liquid nitrogen and liquid oxygen, respectively. The values of yaw angle (θ), combined convection parameter (Ri) and the ratio of buoyancy force parameter (Nc) are varied in the ranges $0 \leq \theta \leq \pi/3$, $-3 \leq Ri \leq 10$ and $0 \leq Nc \leq 1$, respectively. It should be noted that considered values of governing parameters allow one to show the features of liquid behavior and heat and mass transfer.

Further, $\theta = 0$ corresponds to the perfect geometry of a vertical cylinder. Moreover, $\overline{x} = 0$ and $\overline{x} \neq 0$ represent the similarity and nonsimilarity cases, respectively. Additionally, $\varepsilon_1 = u_s/u_e$ and $\varepsilon_2 = w_s/w_e$ are two velocity ratio parameters along chordwise and spanwise directions, respectively.

4.1. Impacts of Combined Convection Parameter and Velocity Ratio Parameter

Figures 2–4 display the influence of combined convection parameter (Ri) and velocity ratio parameters (ε_1 and ε_2) on velocity patterns ($F(\overline{x}, \eta)$ and $S(\overline{x}, \eta)$) and the coefficients of friction at the surface $\left(Re^{1/2}C_f \text{ and } Re^{1/2}\overline{C}_f\right)$ along chordwise and spanwise directions. Increasing magnitude of combined convection characteristics enhances the velocity pattern and the surface drag coefficient in chordwise and spanwise directions. The positive magnitudes of Ri designate the essential impacts of buoyancy force over inertia force.

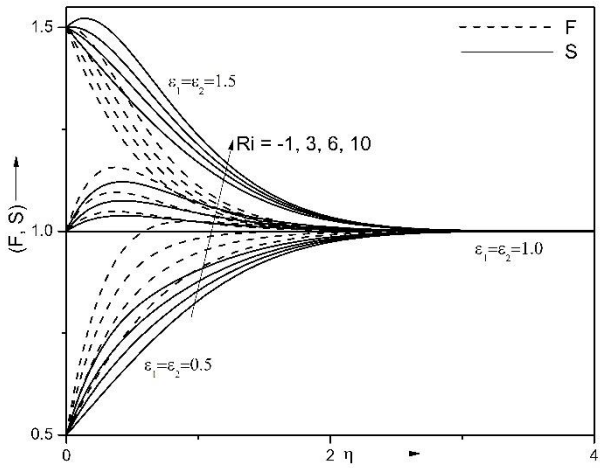

Figure 2. Influence of Ri and velocity ratio parameter (ε_1 and $\varepsilon_{2)}$ on velocity patterns $(F(\overline{x}, \eta), S(\overline{x}, \eta))$ in both chordwise and spanwise direction when $\overline{x} = 0.5$, $\beta_T = 0.1$, $\theta = \pi/6$, $Nc = 0.1$, $\varepsilon_2 = 0.5$, $\beta_C = 0.1$ and $Sc = 160$.

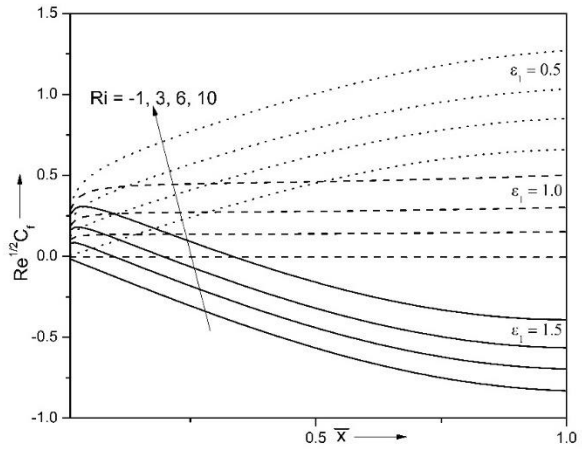

Figure 3. Influence of Ri and ε_1 on surface drag coefficient $\left(Re^{0.5}C_f\right)$ in chordwise direction when $\beta_T = 0.1$, $\theta = \pi/6$, $Nc = 0.1$, $\varepsilon_2 = 0.5$, $\beta_C = 0.1$ and $Sc = 160$.

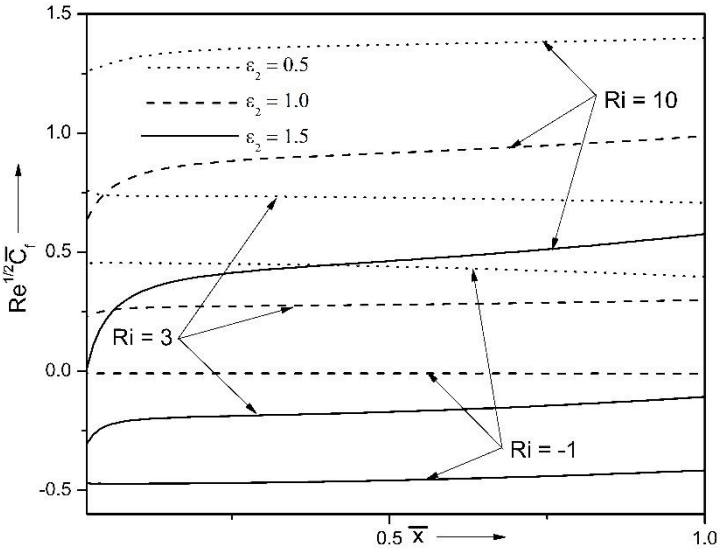

Figure 4. Influence of *Ri* and ε_2 on skin-friction parameter $\left(Re^{0.5}\overline{C}_f\right)$ in spanwise direction when $\beta_T = 0.1$, $\theta = \pi/6$, $Nc = 0.1$, $\varepsilon_1 = 0.8$, $\beta_C = 0.1$ and $Sc = 160$.

Thus, the buoyancy for liquid enhances the liquid motion and simultaneously enhances the liquid's velocity and respective frictions at the surface. Further, for enhancing values of velocity ratio characteristics (ε_1), the velocity profile enhances, while the surface drag coefficient in the chordwise direction diminishes. Moreover, the same behavior is observed for larger values of velocity ratio parameters (ε_2) in the spanwise direction. The physical reason is that, for $\varepsilon_1 < 1$ and $\varepsilon_2 < 1$, the free stream velocity dominates over surface velocity and causes such variations. Moreover, the combined impacts of assisting buoyancy force because of temperature and concentration gradients along with a rise of velocity ratio parameter acts like a favorable pressure gradient which enhances the liquid flow. For $\overline{x} = 0.5$, $Pr = 7.0$, $\beta_T = 0.1$, $\theta = \pi/6$, $Nc = 0.1$, $\varepsilon_1 = \varepsilon_2 = 1.5$, $\beta_C = 0.1$ and $Sc = 160$, the coefficients of friction along chordwise and spanwise directions at the wall are increased by about 22% and 62%, respectively, as *Ri* varies from opposing buoyancy flow case ($Ri = -1$) to assisting buoyancy flow case ($Ri = 3$).

4.2. Impacts of Nonlinear Convection Parameter and Yaw Angle

Figures 5–8 display the influence of velocity ratio characteristics (ε_1) and angle of yaw (θ) on velocity profile $F(\overline{x}, \eta)$ and the coefficients of friction at the surface $\left(Re^{0.5}C_f\right)$ along the chordwise direction. Moreover, the influence of nonlinear convection parameter (β_T) and angle of yaw (θ) on velocity profile $S(\overline{x}, \eta)$ and the coefficient of friction at the surface $\left(Re^{0.5}\overline{C}_f\right)$ along the spanwise direction has been observed. For enhancing values of velocity ratio parameter (ε_1), the velocity pattern increases, while surface drag coefficient in chordwise direction diminishes. The physical reason is that, for $\varepsilon_1 < 1$, the free stream velocity dominates over surface velocity and causes such variations. Further, for the increasing magnitudes of β_T, the velocity patterns and coefficient of friction at the surface increase along the spanwise direction. The larger magnitudes of β_T characterize the greater variation between the plate and the environmental temperature. Therefore, for larger magnitudes of β_T, the larger temperature variation reasons stronger convection and as a result enhances the liquid velocity and the friction between the cylinder and the liquid.

Further, velocity profiles in chordwise and spanwise directions and the skin friction coefficient in chordwise and spanwise directions both increase with the increasing values of yaw angle. Higher values of yaw angle (i.e., the cylinder inclines more) cause pressure increase in the fluid flow and increase fluid velocity, and the inclination of the cylinder causes the enhancement in the surface friction along chordwise and spanwise directions.

Moreover, in Figure 7, at θ = 0, the lines obtained for different values of β_T merge together. For $\bar{x} = 0.5$, Pr = 7.0, Ri = 10.0, β_T = 0.5, Nc = 0.1, ε_1 = 0.8, ε_2 = 0.5, β_C = 0.1 and Sc = 160, the coefficient of friction along spanwise directions at the wall increases by about 50%, as θ varies from $\pi/6$ to $\pi/3$.

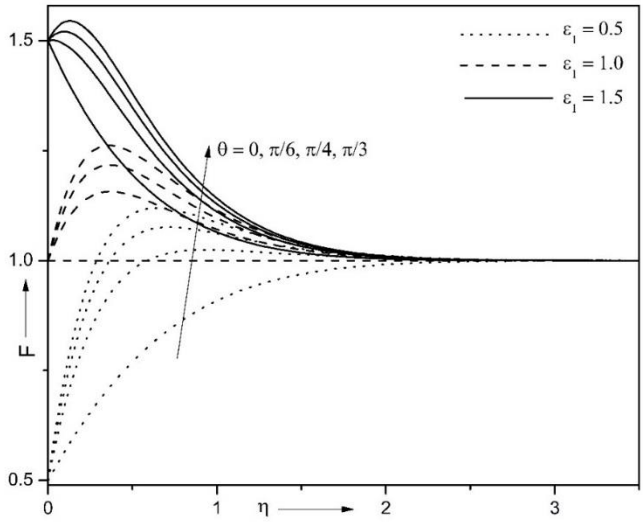

Figure 5. Influence of ε_1 and θ on velocity patterns $F(\bar{x}, \eta)$ in chordwise direction when $\bar{x} = 0.5$, Ri = 10.0, β_T = 0.1, Nc = 0.1, ε_2 = 0.5, β_C = 0.1 and Sc = 160.

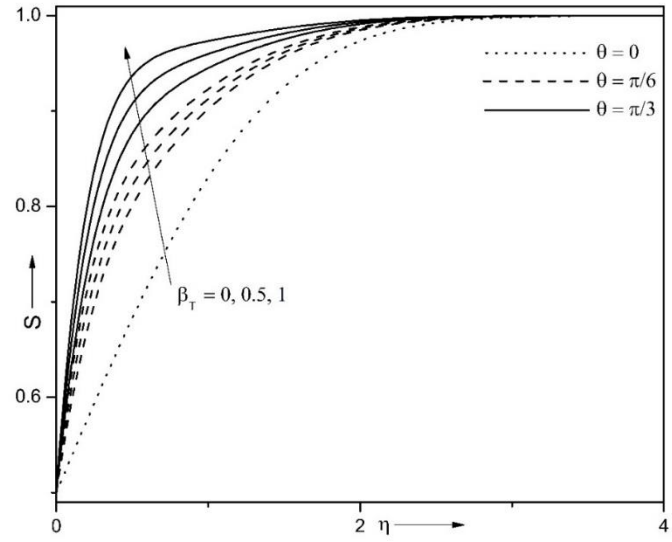

Figure 6. Influence of β_T and θ on velocity patterns $S(\bar{x}, \eta)$ in spanwise direction when $\bar{x} = 0.5$, Ri = 10.0, Nc = 0.1, ε_1 = 0.8, ε_2 = 0.5, β_C = 0.1 and Sc = 160.

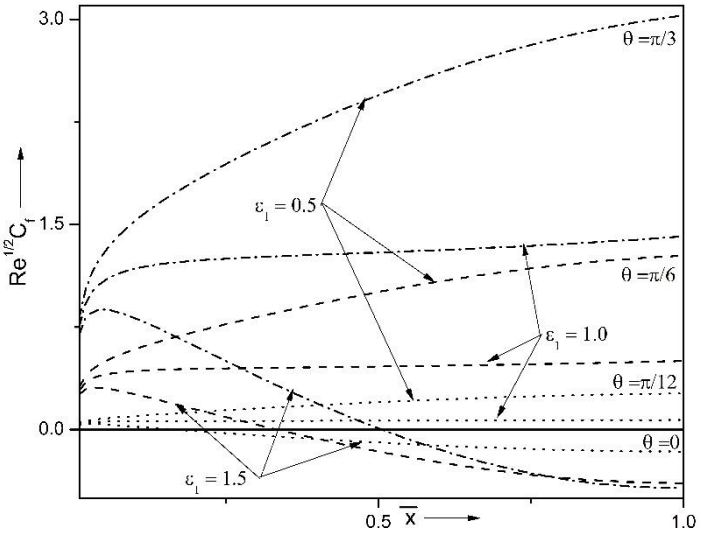

Figure 7. Influence of ε_1 and θ on skin-friction parameter $\left(Re^{0.5}C_f\right)$ in chordwise direction when Ri = 10.0, β_T = 0.1, Nc = 0.1, ε_2 = 0.5, β_C = 0.1 and Sc = 160.

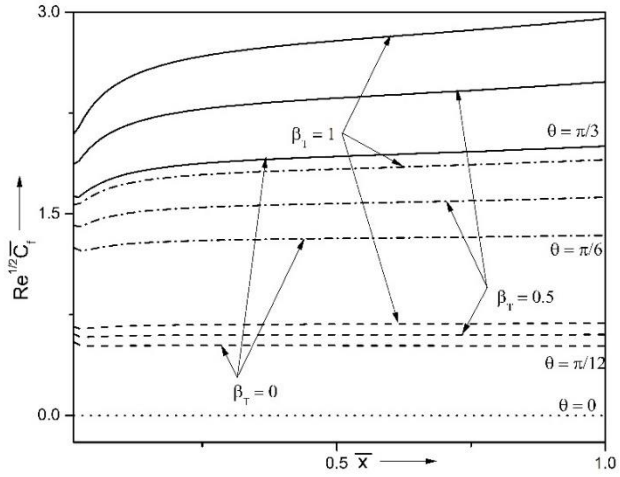

Figure 8. Influence of β_T and θ on surface drag coefficient $\left(Re^{0.5}\overline{C}_f\right)$ in spanwise direction when Ri = 10.0, Nc = 0.1, ε_1 = 0.8, ε_2 = 0.5, β_C = 0.1 and Sc = 160.

4.3. Impacts of Yaw Angle and Schmidt Number

Figures 9 and 10 display the impact of Schmidt number (Sc) as well as angle of yaw (θ) on concentration profile $H(\overline{x}, \eta)$ and the mass transfer rate $\left(Re^{-0.5}Sh\right)$, respectively. It is observed that the concentration profile reduces while the Sherwood number enhances, for the larger Schmidt numbers and angles of yaw. Mass diffusivity reduces for the higher values of Sc. As Sc enhances, the thickness of the concentration boundary layer reduces, and as a result the species concentration profile diminishes. Accordingly, the Sherwood number increases. Further, we observe that there is no deviation for θ = 0 which represents the vertical cylinder, as compared to other yaw angles. For $\overline{x} = 0.5$, Ri = 10.0, β_T = 0.1, Nc = 0.1, ε_1 = 0.8, ε_2 = 0.5, β_C = 0.1 and θ = π/6, the Sherwood number enhances by about 27%, when Sc value is reduced from 340 to 160.

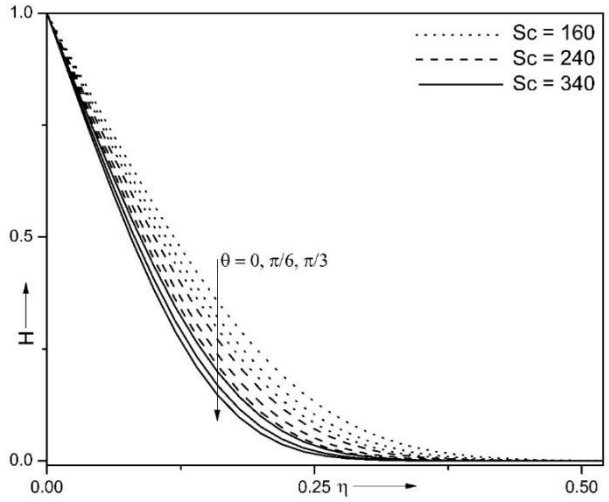

Figure 9. Influence of θ and *Sc* on concentration patterns $H(\overline{x}, \eta)$ when $\overline{x} = 0.5$, $Ri = 10.0$, $\beta_T = 0.1$, $Nc = 0.1$, $\varepsilon_2 = 0.5$, $\beta_C = 0.1$ and $\varepsilon_1 = 0.8$.

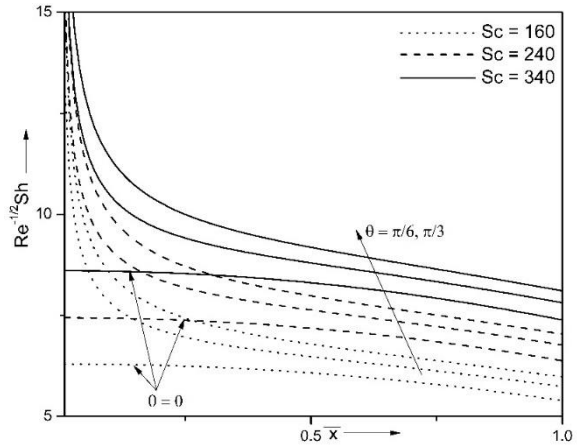

Figure 10. Influence of θ and *Sc* on Sherwood number $\left(Re^{-0.5}Sh\right)$ when $Ri = 10.0$, $\beta_T = 0.1$, $Nc = 0.1$, $\varepsilon_2 = 0.5$, $\beta_C = 0.1$ and $\varepsilon_1 = 0.8$.

4.4. Impact of Yaw Angle and Combined Convection Characteristics

Figures 11 and 12 depict the influence of combined convection parameter (*Ri*) and angle of yaw (θ) on dimensionless temperature pattern $G(\overline{x}, \eta)$ and heat transfer rate $\left(Re^{-0.5}Nu\right)$. Temperature pattern and heat transfer rate are reduced for an enhancing magnitudes of combined convection parameter. The magnitudes $Ri > 0$ illustrate the essential influence of buoyancy force compared to the inertia force. Thus, a rise of the buoyancy impacts illustrates more essential fluid flow that characterizes a reduction of the liquid temperature and an appearance of the cool liquid close to the cylinder's border. This in turn enhances the energy transport strength from the cylinder's border to the liquid. Further, as yaw angle enhances temperature profile and heat transfer rate, for enhancing magnitudes of combined convection parameter, we observe the curves obtained by varying the yaw angle; the curves overlap into a single curve with irrespective values of combined convection parameter.

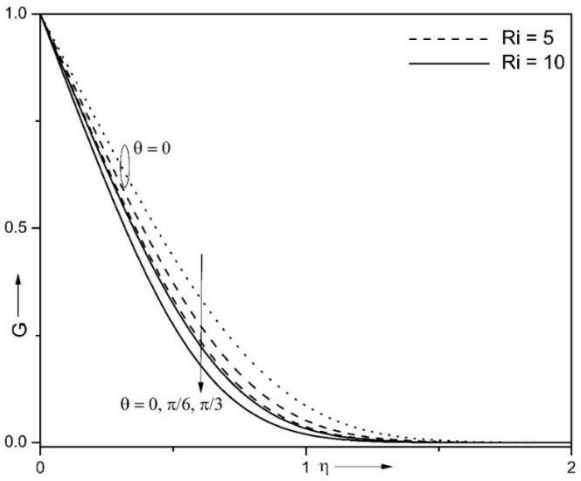

Figure 11. Influence of *Ri* and θ on temperature patterns $G(\overline{x}, \eta)$ when $\overline{x} = 0.5$, $\beta_T = 0.1$, $Nc = 0.1$, $\varepsilon_1 = 0.8$, $\varepsilon_2 = 0.5$, $\beta_C = 0.1$ and $Sc = 160$.

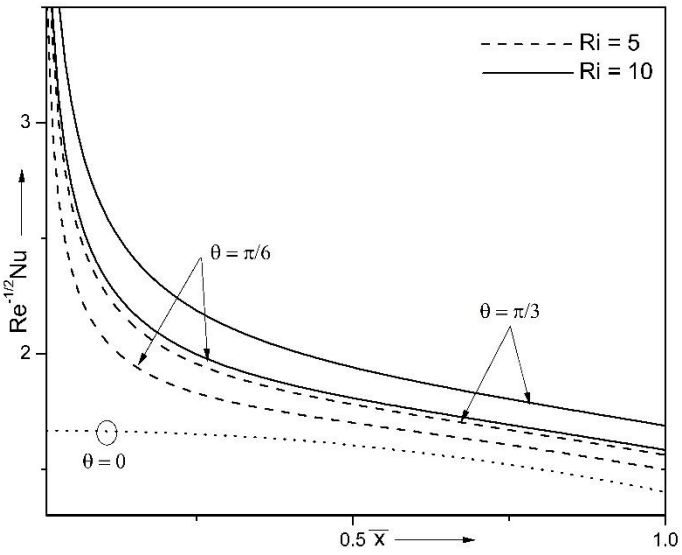

Figure 12. Influence of *Ri* and θ on heat transfer rate $\left(Re^{-0.5}Nu\right)$ when $\beta_T = 0.1$, $Nc = 0.1$, $\varepsilon_1 = 0.8$, $\varepsilon_2 = 0.5$, $\beta_C = 0.1$ and $Sc = 160$.

Further, we observe that there is no deviation for θ = 0 which represents the vertical cylinder, as compared to other yaw angles. Moreover, at $\overline{x} = 0.5$ and $Ri = 10.0$, as yaw angle enhances from θ = π/6 to θ = π/3, Nusselt number increases approximately about 7%.

Velocity profile $F(\overline{x}, \eta)$ is compared with the already existing results of Eswara and Nath [40] for a particular case by assuming $A = 0$, $Ec = 0$, θ = 0. The results are found in an excellent agreement and the comparisons are shown in Figure 13.

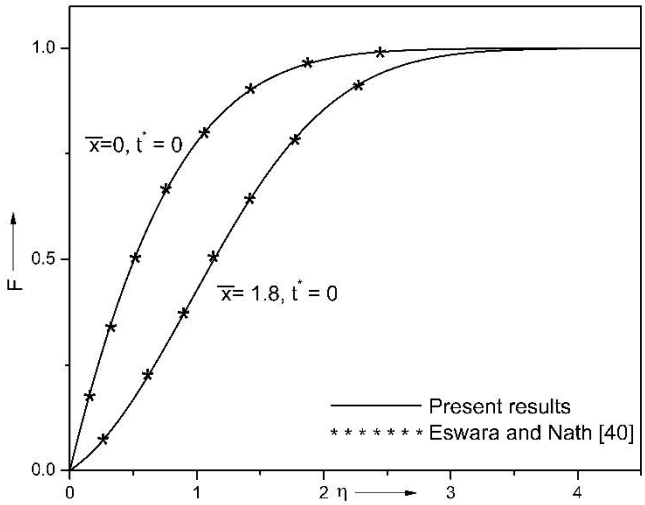

Figure 13. Comparison of velocity profile $F(\bar{x}, \eta)$ with the particular case of flow over cylinder for $\theta = 0$, $Ec = 0$ and $A = 0$.

Table 1 demonstrates the variations of friction parameter at the yawed cylinder along chordwise direction, Nusselt and Sherwood numbers, for various magnitudes of yaw angle. From the Table 1, it is found that the surface drag coefficient, Nusselt and Sherwood numbers are raised for increasing yaw angles. The friction parameter, rates of heat transfer and mass transfer are enhanced by about 31%, 2% and 1%, respectively, at $\bar{x} = 0.5$, as yaw angle varies from $\pi/12$ to $\pi/6$.

Table 1. Surface drag coefficient along chordwise direction $\left(Re^{0.5}C_f\right)$, heat transfer rate $\left(Re^{-0.5}Nu\right)$ and mass transfer rate $\left(Re^{-0.5}Sh\right)$ values, for different values of yaw angle ($\theta = 0$ to $\theta = \pi/3$) when $Ri = 10.0$, $\beta_T = 0.1$, $Nc = 0.1$, $\varepsilon_1 = 0.8$, $\varepsilon_2 = 0.5$, $\beta_C = 0.1$ and $Sc = 160$.

Yaw Angle (θ)	$\lvert Re^{0.5}C_f \rvert$	$\lvert Re^{-0.5}Nu \rvert$	$\lvert Re^{-0.5}Sh \rvert$
0	0	0.94430	4.41621
$\pi/12$	0.12140	0.94281	4.42190
$\pi/6$	0.68785	0.95536	4.43383
$\pi/3$	3.10383	0.96857	4.45684

5. Conclusions

This research considers the double-diffusive combined convection around a moved yawed cylinder. In that, the influence of varying strength of yaw angle, mixed convection and nonlinear convection characteristics on the velocity patterns and skin friction coefficients in chordwise and spanwise directions, nondimensional temperature, concentration profile, mass and heat transfer rates are analyzed employing different graphs. Taking into account this detailed analysis, the obtained outcomes are detailed as follows:

- Velocity profiles can be enhanced, while the coefficients of friction at the surface diminish, for increasing values of velocity ratio parameters in spanwise and chordwise directions.
- For enhancing magnitudes of nonlinear convection coefficient, the velocity profile and the skin friction parameter in spanwise direction are increased.
- Concentration profile diminishes, while the Sherwood number enhances, for increasing values of Schmidt number and yaw angle.
- Velocity profiles in spanwise and chordwise directions and skin friction coefficient at the border in chordwise and spanwise directions are enhanced with growing values of yaw angle.

– Increasing magnitude of combined convection characteristics, enhancing the velocity profiles and surface drag coefficient in spanwise and chordwise directions.

Author Contributions: Conceptualization, P.M.P., H.F.S. and M.A.S.; methodology, P.M.P. and H.F.S.; formal analysis, P.M.P., H.F.S. and M.A.S.; investigation, P.M.P., H.F.S. and M.A.S.; writing—original draft preparation, P.M.P., H.F.S. and M.A.S.; writing—review and editing, P.M.P., H.F.S. and M.A.S.; supervision, P.M.P. and M.A.S. All authors have read and agreed to the published version of the manuscript.

Funding: This research of P.M. Patil and H.F. Shankar was funded by University Grant's Commission, New-Delhi, grant number F. 16-6/(DEC.2018)/2019(NET/CSIR)940 dated 24-07-2019.

Institutional Review Board Statement: Not applicable.

Informed Consent Statement: Not applicable.

Data Availability Statement: All data are presented in this article.

Acknowledgments: This research of M.A. Sheremet was supported by the TPU development program.

Conflicts of Interest: The authors declare no conflict of interest.

Nomenclature

C	Species Concentration:
C_s	species concentration at the surface
C_∞	ambient species concentration
D_B	Brownian diffusion coefficient ($m^2\ s^{-1}$)
F	dimensionless stream function
G	nondimensional temperature
Gr	Grashof number
G	acceleration due to gravity ($m\ s^{-2}$)
H	nondimensional concentration
Nc	buoyancy ratio
Nu	Nusselt number
Pr	Prandtl number
R	radius of the cylinder (m)
Ri	mixed convection parameter
Sc	Schmidt number
Sh	Sherwood number
T	temperature (K)
T_s	temperature at the surface (K);
T_∞	ambient temperature (K)
U	x-velocity ($m\ s^{-1}$)
u_∞	free stream velocity ($m\ s^{-1}$)
V	y-velocity ($m\ s^{-1}$)
w	z-velocity ($m\ s^{-1}$)
x, y and z	curvilinear coordinates (m)
Greek symbols	
β_1, β_2	linear and nonlinear thermal expansion parameters (K^{-1})
β_3, β_4	linear and nonlinear thermal expansion parameters of liquid hydrogen
β_C	nonlinear concentration convection coefficient for liquid hydrogen
β_T	nonlinear temperature convection coefficient
$\Delta\overline{x}$, $\Delta\eta$	step size for $\overline{x}$ and η coordinates
ε_1	velocity ratio parameter along chordwise direction
ε_2	velocity ratio parameter along spanwise direction
$\overline{x}, \eta$	transformed variables

θ	yaw angle
ν	kinematic viscosity ($m^2\ s^{-1}$)
ψ	dimensionless stream function
Subscripts	
$\overline{x}, \eta$	denote the partial derivatives with respect to these variables
e	indicates the condition at the boundary layer edge
w	indicates the condition at the wall
∞	indicates the condition at the mainstream.

References

1. Saha, S.; Hasan, M.N.; Khan, I.A. Double diffusive mixed convection heat transfer inside a vented square cavity. *Chem. Eng. Res. Bull.* **2009**, *13*, 17–24. [CrossRef]
2. Chamkha, A.J.; Aly, A.M.; Raizah, Z.A.S. Double diffusion MHD free convective flow along a sphere in the presence of a homogeneous chemical reaction and Soret and Dufour effects. *Appl. Comput. Math.* **2017**, *6*, 34–44. [CrossRef]
3. Patil, P.M.; Doddagoudar, S.H.; Hiremath, P.S. Impacts of surface roughness on mixed convection nanoliquid flow with liquid hydrogen/nitrogen diffusion. *Int. J. Numer. Methods Heat Fluid Flow* **2019**, *29*, 2146–2174. [CrossRef]
4. Reddy, L.R.; Raju, M.C.; Raju, G.S.S. Unsteady MHD free convection flow characteristics of a viscoelastic fluid past a vertical porous plate. *Int. J. Appl. Sci. Eng.* **2016**, *14*, 69–85.
5. Pail, P.M.; Pop, I. Effects of surface mass transfer on unsteady mixed convection flow over a vertical cone with chemical reaction. *Heat Mass Transf.* **2011**, *47*, 1453–1464.
6. Patil, P.M.; Kulkarni, M.; Hiremath, P.S. Effects of surface roughness on mixed convective nanofluid flow past an exponentially stretching permeable surface. *Chin. J. Phys.* **2020**, *64*, 203–218. [CrossRef]
7. Prasad, K.V.; Vajravelu, K.; Vaidya, H.; Datti, P.S. Axisymmetric flow over a vertical slender cylinder in the presence of chemically reactive species. *Int. J. Appl. Comput. Math.* **2017**, *3*, 663–678. [CrossRef]
8. Vajravelu, K.; Sastri, K.S. Fully developed laminar free convection flow between two parallel vertical walls. *Int. J. Heat Mass Transf.* **1977**, *20*, 655–660. [CrossRef]
9. Bhargava, R.; Agarwal, R.S. Fully developed free convection flow in a circular pipe. *Indian J. Pure Appl. Math.* **1979**, *10*, 357–365.
10. Motsa, S.S.; Awad, F.G.; Khumalo, M. Nonlinear nanofluid flow overheated vertical surface with sinusoidal wall temperature variations. *Abstr. Appl. Anal.* **2014**, *2014*, 408230. [CrossRef]
11. Muthukumaran, C.; Bathrinathan, K. Mathematical modeling of mixed convection boundary layer flows over a stretching sheet with viscous dissipation in presence of suction and injection. *Symmetry* **2020**, *12*, 1754. [CrossRef]
12. Halim, N.A.; Noor, N.F.M. Mixed convection flow of Powell–Eyring nanofluid near a stagnation point along a vertical stretching sheet. *Mathematics* **2021**, *9*, 364. [CrossRef]
13. Alsabery, A.I.; Ghalambaz, M.; Armaghani, T.; Chamkha, A.; Hashim, I.; Pour, M.S. Role of rotating cylinder toward mixed convection inside a wavy heated cavity via Two-Phase nanofluid concept. *Nanomaterials* **2020**, *10*, 1138. [CrossRef]
14. Khashiie, N.S.; Md Arifin, N.; Pop, I. Mixed convective stagnation point flow towards a vertical Riga plate in hybrid Cu-Al_2O_3/water nanofluid. *Mathematics* **2020**, *8*, 912. [CrossRef]
15. Liang, H.; Duan, R. Effects of lateral end plates on flow crossing a yawed circular cylinder. *Appl. Sci.* **2019**, *9*, 1590. [CrossRef]
16. King, R. Vortex excited oscillations of yawed circular cylinders. *J. Fluids Eng.* **1977**, *99*, 495–501. [CrossRef]
17. Revathi, G.; Saikrishnan, P.; Chamkha, A.J. Non-similar solutions for unsteady flow over a yawed cylinder with non-uniform mass transfer through a slot. *Ain Shams Eng. J.* **2014**, *5*, 1199–1206. [CrossRef]
18. Najafi, L.; Firat, E.; Akilli, H. Time-averaged near-wake of a yawed cylinder. *Ocean. Eng.* **2016**, *113*, 335–349. [CrossRef]
19. Snarski, S.R. Flow over yawed circular cylinders: Wall pressure spectra and flow regimes. *Phys. Fluids* **2004**, *16*, 344–359. [CrossRef]
20. Sears, W.R. The boundary layer of yawed cylinders. *J. Aeronaut. Sci.* **1948**, *15*, 49–52. [CrossRef]
21. Thapa, J.; Zhao, M.; Zhou, T.; Cheng, L. Three-dimensional simulation of vortex shedding flow in the wake of a yawed circular near a plane boundary at a Reynolds number of 500. *Ocean. Eng.* **2014**, *87*, 25–39. [CrossRef]
22. Gupta, T.R.; Sarma, G.N. Effect of cross flow in unsteady flow past a yawed infinite cylinder. *Indian J. Pure Appl. Math.* **1975**, *6*, 1047–1065.
23. Bucker, D.; Lueptow, R.M. The boundary layer on a slightly yawed cylinder. *Exp. Fluids* **1998**, *25*, 487–490. [CrossRef]
24. Subhashini, S.V.; Takhar, H.S.; Nath, G. Non-uniform multiple slot injection (suction) or wall enthalpy into a compressible flow over a yawed cylinder. *Int. J. Therm. Sci.* **2003**, *42*, 749–757. [CrossRef]
25. Roy, S. Non uniform mass transfer wall enthalpy into a compressible flow over yawed cylinder. *Int. J. Heat Mass Transf.* **2001**, *44*, 3017–3024. [CrossRef]
26. Roy, S.; Saikrishnan, P. Non-uniform slot injection (suction) into water boundary layer flow past yawed cylinder. *Int. J. Eng. Sci.* **2004**, *42*, 2147–2157. [CrossRef]
27. Saikrishnan, P. Boundary layer flow over a yawed cylinder with variable viscosity role of non-uniform double slot suction (injection). *Int. J. Numer. Methods Heat Fluid Flow* **2012**, *22*, 342–356.
28. Marshall, J.S. Wake dynamics of a yawed cylinder. *J. Fluid Eng.* **2003**, *125*, 97–103. [CrossRef]

29. Vakil, A.; Green, S.I. Drag and lift coefficients of inclined finite circular cylinders at moderate Reynolds numbers. *Comput. Fluids* **2009**, *38*, 1771–1781. [CrossRef]
30. Patil, P.M.; Roy, S. Corrigendum of "Mixed convection flow past a yawed cylinder" [ICHMT 114 (2020) 104582]. *Int. Commun. Heat Mass Transf.* **2021**, *124*, 105246. [CrossRef]
31. Chiu, W.S.; Lienhard, J.H. On real fluid flow over yawed circular cylinders. *J. Fluid Eng.* **1967**, *89*, 851–857. [CrossRef]
32. Patil, P.M.; Shankar, H.F.; Hiremath, P.S.; Momoniat, E. Nonlinear mixed convective nanofluid flow about a rough sphere with the diffusion of liquid hydrogen. *Alex. Eng. J.* **2021**, *60*, 1043–1053. [CrossRef]
33. Patil, P.M.; Ramane, H.S.; Hindasageri, V.; Momoniat, E. Influence of mixed convection in an exponentially decreasing external flow velocity. *Int. J. Heat Mass Transf.* **2017**, *104*, 392–399. [CrossRef]
34. Patil, P.M.; Shashikant, A.; Hiremath, P.S. Diffusion of liquid hydrogen and oxygen in nonlinear mixed convection nanofluid flow over vertical cone. *Int. J. Hydrog. Energy* **2019**, *44*, 17061–17071. [CrossRef]
35. Schlichting, H.; Gersten, K. *Boundary Layer Theory*; Springer: New York, NY, USA, 2000.
36. Patil, P.M.; Shashikant, A.; Roy, S.; Hiremath, P.S. Mixed convection flow past a yawed cylinder. *Int. Commun. Heat Mass Transf.* **2020**, *114*, 104582. [CrossRef]
37. Inouye, K.; Tate, A. Finite difference version Quasilinearization applied to boundary layer equations. *AIAA J.* **1974**, *12*, 558–560. [CrossRef]
38. Singh, P.J.; Roy, S. Unsteady mixed convection from a rotating vertical slender cylinder in an axial flow. *Int. J. Heat Mass Transf.* **2008**, *51*, 1423–1430. [CrossRef]
39. Varga, R.S. *Matrix Iterative Analysis*; Prentice-Hall: Englewood Cliffs, NJ, USA, 2000.
40. Eswara, E.T.; Nath, G. Unsteady nonsimilar two-dimensional and axisymmetric water boundary layers with viscosity and Prandtl number. *Int. J. Eng. Sci.* **1994**, *32*, 267–279. [CrossRef]